Research Article

Highly sensitive phototransistors based on two-dimensional GaTe nanosheets with direct bandgap

Pingan Hu[1] (✉), Jia Zhang[1], Mina Yoon[2], Xiao-Fen Qiao[3], Xin Zhang[3], Wei Feng[1], Pingheng Tan[3] (✉), Wei Zheng[1], Jingjing Liu[1], Xiaona Wang[1], Juan C. Idrobo[2], David B. Geohegan[2], and Kai Xiao[2] (✉)

[1] *Key Lab of Microsystem and Microstructure, Harbin Institute of Technology, Ministry of Education, No. 2 Yikuang Street, Harbin, 150080, China*
[2] *Center for Nanophase Materials Sciences, Oak Ridge National Laboratory, One Bethel Valley Road, Oak Ridge, TN, 37831, USA*
[3] *State Key Laboratory of Superlattices and Microstructures, Institute of Semiconductors, Chinese Academy of Sciences, Beijing 100083, China*

ABSTRACT

Highly sensitive phototransistors based on two-dimensional (2D) GaTe nanosheet have been demonstrated. The performance (photoresponsivity, detectivity) of the GaTe nanosheet phototransistor can be efficiently adjusted by using the applied gate voltage. The devices exhibit an ultrahigh photoresponsivity of 274.3 AW^{-1}. The detectivity of 2D GaTe devices is ~10^{12} Jones, which surpasses that of currently-exploited InGaAs photodetectors (10^{11}–10^{12} Jones). To reveal the origin of the enhanced photocurrent in GaTe nanosheets, theoretical modeling of the electronic structures was performed to show that GaTe nanosheets also have a direct bandgap structure, which contributes to the promotion of photon absorption and generation of excitons. This work shows that GaTe nanosheets are promising materials for high performance photodetectors.

1 Introduction

Two-dimensional (2D) semiconducting materials are attracting great interest for applications in next-generation electronics and optoelectronics [1–7]. Many layered 2D crystals with different properties have been explored, ranging from insulating h-BN and semimetallic graphene to semiconducting layered metal chalcogenides (e.g. MoS_2, WS_2, GaSe, GaS, and In_2Se_3) [8–13]. Graphene, the first 2D material to undergo widespread application development, has proven to be a promising material for ultrafast electronics and wideband, high speed photodetectors due to its ultrahigh carrier mobility, wide-band absorption and short carrier lifetime [14]. For example, graphene field-effect transistors (FETs) have been operated

---

with a 100-GHz cutoff frequency, which is much higher than that of Si metal–oxide–semiconductor FETs [15]. In addition, graphene photodetectors have also been demonstrated for ultra-wide band (300 nm–6 μm) operation, far exceeding the bandwidth capabilities of other current photodetectors [16, 17]. Moreover, by introducing electron trap centers to create a bandgap in graphene, Wang et al. demonstrated a high photoresponsivity of 8.61 AW^{-1} in pristine monolayer graphene [18]. However, pristine monolayer graphene is inherently a zero-bandgap material, with much lower light absorption and shorter carrier lifetimes. Therefore, 2D layered materials with bandgaps, such as metal chalcogenides, are better candidates for photodetectors. Recent studies have demonstrated that single-layer or multilayer MoS_2-based photodetectors have tunable spectral photoresponse [8, 19] and can be ultrasensitive, with photoresponsivities reaching 880 AW^{-1}. This 10^6-fold improvement in photoresponse over previous reports for monolayer MoS_2 phototransistors resulted both from improvements in the mobility of the MoS_2 as well as in the contact quality and positioning in fabrication of the devices [19]. These results exemplify the promise of inorganic 2D nanosheets as semiconductor materials for applications in high performance electronics and optoelectronics.

2D semiconducting nanosheets with direct bandgaps are of primary interest for optoelectronic applications such as photodetectors, because they are efficient light absorbers, ultrathin and processable. 2D materials with indirect bandgaps, such as transition metal dichalcogenides (TMDCs) such as MoS_2 and WS_2, can sometimes develop direct bandgaps as their thickness approaches a monolayer. However, the controllable production of monolayer TMDCs is currently difficult to achieve, although the growth of monolayer MoS_2 films containing small crystalline grains about ~100 μm in size have been reported [20, 21]. So it would greatly facilitate scientific explorations if large-area 2D nanosheets could be exfoliated from both direct- and indirect-bandgap layered bulk compounds. Besides graphene and MoS_2 nanosheets, III–VI group metal layered materials such as GaSe, GaS, and In_2Se_3 also have shown interesting optoelectronic properties. For example, recently we have demonstrated UV photodetectors based on few-layer GaSe and GaS nanosheets

with strong light absorption, exhibiting a responsivity of 2.8 AW^{-1} and 19.2 AW^{-1} respectively [10, 11]. However, these materials still retain an indirect bandgap in monolayer exfoliated sheets, unlike transition metal dichalcogenides, lowering the efficiency of photon absorption or emission.

GaTe is within the III–VI group of layered metal chalcogenides with each layer consisting of Te–Ga–Ga–Te repeating units stacked along the c-axis. GaTe has a monoclinic layered structure with the C2/m space-group symmetry in which only two thirds of the Ga–Ga bonds are perpendicular to the layer planes and the others are in the layer plane. However, other III–VI layered materials such as GaSe and GaS forms a four-sheet intralayer stacking pattern and all the Ga-Ga are perpendicular to the layer plane [22, 23]. Moreover, unlike bulk GaSe and GaS with indirect bandgaps of above 2.0 eV [22], bulk GaTe has a relatively small direct bandgap of ~1.60 eV with strong excitonic absorption even at room temperature [23, 24]. Additionally, GaTe exhibits high carrier mobilities and long carrier lifetimes [24]. For these reasons, bulk GaTe crystals have shown excellent electronic and optical properties and therefore have been applied in optoelectronic devices, radiation detectors and solar cells [24–26]. However, while the properties of 2D nanosheets of III–VI 2D layered metal chalcogenides have recently been reported in the Refs. [10, 11], the electrical and optical properties of GaTe nanosheets are largely unexplored.

Here, we demonstrate an ultrasensitive photodetector based on exfoliated 2D GaTe nanosheets. We find that the Raman scattering and photoluminescence (PL) of the exfoliated GaTe nanosheets exhibit a strong thickness dependence. The performance (photoresponsivity, detectivity) of the GaTe ultrathin layer phototransistor can be tuned by varying the applied gate voltage. Our devices show a high photoresponsivity between 254–700 nm with a maximum external photoresponsivity of 274.1 AW^{-1} at a wavelength of 490 nm, which is 10^4 times higher than those of pristine graphene photodetectors (0.1 AW^{-1}; Quantum yield: 6%–16% [13]). In addition, they show a high detectivity (D^*) of ~10^{12} Jones, which is comparable to existing InGaAs devices (D^* ~10^{12} Jones) [27]. Theoretical modeling of the electronic structures of the

GaTe nanosheets indicates that their direct bandgap contributes to the enhancement of photon absorption compared to similar layer thicknesses of the indirect bandgap GaSe and GaS nanosheets.

2   Experimental

2.1   Material preparation and characterization

The GaTe crystals were synthesized by a modified Bridgman method. Pure 5N (99.999%) gallium chunks and 5N telluride pellets in the proportion about 1:1 were mixed into a graphite crucible, after which the crucible was placed in a quartz tube. During the synthesis of GaTe crystals ,the reaction site of the tube was heated to 900 ℃ in an argon environment under a low vacuum conditions and kept for 1 h. Few-layered GaTe sheets were peeled by Scotch tape from the bulk GaTe and deposited onto cleaned Si/SiO₂ (300 nm). The composition and structure of few-layer GaTe were characterized and analyzed by scanning electron microscopy (SEM, JSM-6301F), transmission electron microscopy (TEM, JEOL-2010F) with an energy-dispersion X-ray spectroscopy (EDS) attachment. The z-contrast images were obtained on an aberration-corrected Nion UltraSTEM scanning transmission electron microscope (STEM) operating at 100 kV, using a half-angle range of the annular dark field detector of 86 to 200 mrad. The thicknesses were determined by atomic force microscopy (AFM). The bulk GaTe crystals and few-layer GaTe nanosheets were characterized by photoluminescence (PL) and Raman spectroscopy at 77 K using a Raman spectroscopy (Horiba-Jobin Yvon HR800), equipped with a liquid nitrogen cooled CCD at the excitation line of 638 nm.

2.2   Device fabrication and characterization

For FET device fabrication, GaTe sheets were deposited onto cleaned Si/SiO₂ (300 nm) substrates. Metal electrodes with a 5-nm thick Cr layer and 50-nm thick Au layer were fabricated using a shadow mask by e-beam deposition. The devices were then annealed at 200 ℃ to decrease contact resistance. Electrical measurements of these devices were performed by using a semiconductor analyzer (Keithley 4200 SCS) combined with a Lakeshore probe station. The photo-current measurements were carried out using a Lakeshore probe station and an HP 4140B Semiconductor Parameter Analyzer. The intensities of incident beams were checked by a power and energy meter (Model 372, Scientech).

3   Results and discussion

Ultrathin GaTe nanosheets on Si/SiO₂ (300 nm) substrates were characterized by SEM, AFM, TEM, micro-Raman spectroscopy, and photoluminescence spectroscopy. Figure 1(a) shows a typical SEM image of a GaTe nanosheet, presenting a 2D morphology indicative of a layered material. Figure 1(b) shows a typical low-magnification TEM image of GaTe nanosheets, as well as an atomic-resolution scanning transmission electron microscopy (AR-STEM) image (Fig. 1(c)) from which a lattice spacing of 0.29 nm can be directly measured. In Fig. 1(c) we present a selected area electron diffraction (SAED) pattern which indicates that the GaTe nanosheets have a monoclinic crystal structure. The thickness of the exfoliated GaTe nanosheets was measured by AFM to be within a thickness range of 1–60 nm. Figure 1(d) is a typical AFM image of a GaTe nanosheet and the cross sectional height in Fig. 1(e) reveals the thickness of the GaTe exfoliated nanosheets in this case is ~3 nm, implying four-layer GaTe.

Raman spectroscopy is a powerful characterization method to understand the structure of layered materials. Raman spectra of bulk GaTe with freshly cleaved surfaces are presented in Fig. 1(f). Two prominent peaks at 112 cm^{-1} and 117 cm^{-1} are observed under the condition where the incident light is parallel (VV) to the scattered light. Other peaks with weak intensity under the VV configuration are located at 67 cm^{-1}, 156 cm^{-1}, 181 cm^{-1}, 212 cm^{-1}, 272 cm^{-1}, and 288 cm^{-1}. However, these modes totally disappear when the incident light is perpendicular (VH) to the scattered light, while instead three new peaks at 167 cm^{-1}, 172 cm^{-1}, and 180 cm^{-1} appear. GaTe belongs to the space group C2/m (point group C_{2h}), with a unit cell consisting of six GaTe molecules (12 atoms). The long-wavelength phonons are described by the irreducible representations of the C_{2h} point group as $\Gamma = 12A_g + 6B_g + 6A_g + 12B_u$, where $A_u + 2B_u$ are
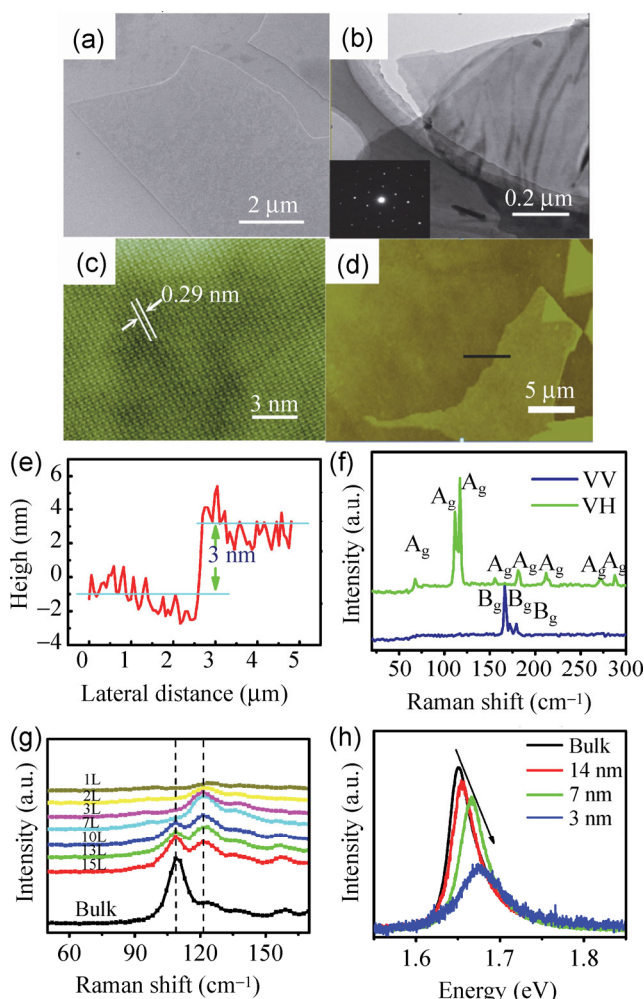
Figure 1 Characterization of GaTe nanosheets including (a) a typical SEM image; (b) a typical low resolution TEM image (inset is the selected area diffraction pattern); (c) z-contrast STEM image showing the atomic structure of a GaTe nanosheets; (d) a typical AFM image of a GaTe nanosheet, and (d) corresponding step height profile from the AFM line scan as indicated in (e) showing a thickness of 3 nm; (f) Raman spectra of bulk GaTe with fresh surface at 77 K under VH and VV configurations, where VH (VV) refers that the incident light is perpendicular (parallel) to the scattered light; (g) Raman spectra of GaTe flakes with different thickness. (h) PL spectra of GaTe nanosheets with different thickness.

acoustic, $5A_u + 10B_u$ are infrared active (IR), and $12A_g + 6B_g$ are Raman active modes. According to the Raman tensors of A_g and B_g, [28] the modes only present under VV configuration are denoted by A_g while the modes only present under VH configuration are denoted by B_g, as shown in Fig. 1(f). Figure 1(g) shows Raman spectra of GaTe nanosheets with different thicknesses. No obvious frequency shifts were observed with different thicknesses, which is totally different from the results reported so far for other 2D semiconductor nanosheets, such as MoS_2 and GaS. The Raman signal from the in-plane E^1_{2g} and the out-of-plane A_{1g} in MoS_2 or GaS nanosheets show a strong thickness dependence [29, 30]. The invariance of the Raman frequency in GaTe nanosheets with layer number is possibly due to the comparatively long-range Coulombic interactions and weaker interlayer interactions within GaTe layers. However, the intensity ratio of the mode at 112 cm^{-1} to that at 117 cm^{-1} increases with layer thickness. Figure 1(g) shows that the linewidth of the Raman modes significantly increase as the layer thickness decreases. This may indicate that the phonon modes in GaTe multilayers are strongly anharmonic with an enhancement of phonon–phonon scattering as the thickness is reduced.

Figure 1(h) shows the room temperature PL spectrum of bulk and GaTe nanosheets with different thicknesses, obtained using an excitation wavelength of 638 nm. The PL intensity decreases with reduced thickness. The PL peak corresponds to the direct bandgap of GaTe sheets. As shown in Fig. 1(h), the bandgap of GaTe nanosheets shows thickness dependence, as the PL peak varies from 1.650 eV to 1.674 eV with decreasing thickness down to 3 nm. This corresponds well to Harper et al.'s finding that the energy gap increases as $1/d^2$ due to quantum size effects when the thickness of a semiconductor crystal is sufficiently reduced [31].

To explore the electrical and photoelectrical properties of GaTe nanosheets, Cr/Au (5/50 nm) electrodes were made on the two ends of GaTe nanosheets deposited onto doped silicon substrates covered with 300-nm-thick SiO_2. Figure 2(a) and Figure 2(b) show a typical transfer curve and output curve of a GaTe nanosheet transistor at room temperature, respectively, indicating a p-type behavior which is consistent with previous reports [21]. We estimate the carrier mobility of the devices by using the equation: $\mu = L/ (W \times C_i \times V_{ds}) \times dI_{ds}/dV_{g},$ where L = 10 μm is the channel length and the channel width W = 40 μm. $C_i = 1.15 \times 10^{-8}$ F/cm^{-2} is the capacitance between the channel and the back gate per unit area, $C_i = \varepsilon_o\varepsilon_r/d$; ε_r (3.9) and d (300 nm) are the dielectric constant and thickness of SiO_2, respectively. The calculated mobility of the devices is 4.6 cm$^2\cdot$V$^{-1}\cdot$s^{-1}. Our devices therefore show higher carrier mobilities than monolayer MoS_2 or GaSe on similar SiO_2/Si substrates [32, 33].
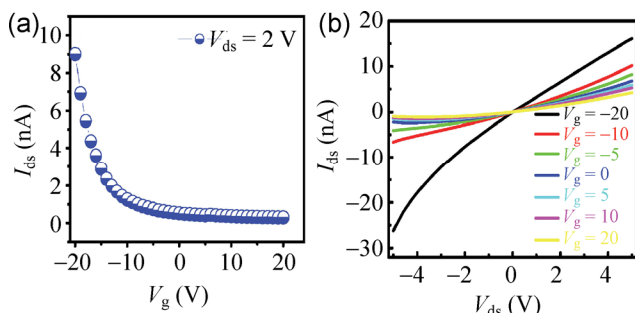
Figure 2 Electrical properties of a GaTe nanosheet transistor. (a) Transfer curve, (b) output curve.

To measure the photoresponse behavior of ultrathin GaTe nanosheets devices on SiO_2/Si substrates, monochromatic light illumination was directed vertically onto devices consisting of two Cr/Au electrodes and a 10-μm length channel, with a 15-μm wide GaTe nanosheet (depicted in Figs. 3(a) and 3(b)). The thickness of the GaTe nanosheets in this device is ~4 layers as estimated by AFM measurements. Electrical characterization was recorded with a fixed illumination intensity of 0.29 mW·cm^{-2} under different illumination wavelengths ranging from 710 nm to 254 nm (Fig. 3(c)). The device shows a wide spectral response to light from the ultraviolet through the visible. The I_{ds}–V_{ds} curves shown in Fig. 3(c) are linear, indicating an Ohmic contact, but also exhibiting a significant increase of source–drain current by several orders of magnitude as the device is illuminated. Accordingly, the photocurrents I_{ph} ($I_{ph} = I_{illumination} - I_{dark}$) also increase with the bias voltage V_{ds}, which is due to the increase in carrier drift velocity and the related decrease of carrier transit time T_t.

The dependence of photocurrent on the gate bias was explored under illumination of 254 nm and 490 nm with a fixed illumination intensity of 0.29 mW·cm^{-2} and bias voltage of 2 V (shown in Fig. 3(d)). As the device is illuminated, the OFF state current increases from ~8 pA to ~40 pA for 490 nm, and from ~8 pA to 1.6 nA for 254 nm. In both cases, the device current in both OFF and ON states increases across the whole gate voltage range employed. This indicates that photocurrent dominates over thermionic and tunneling currents across the entire operating range of gate voltages.
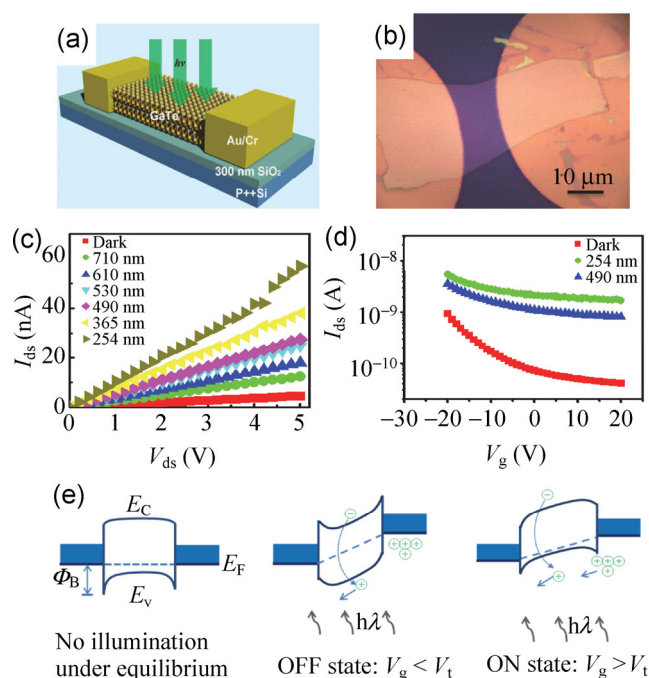
The observed behavior of our GaTe nanosheet

Figure 3 Photoinduced response of GaTe nanosheet phototransistor. (a) Schematic drawing of photodetector based on GaTe nanosheets; (b) a typical image of the GaTe nanosheet devices; (c) drain–source (I_{ds}–V_{ds}) characteristics of the device under different illumination wavelength; (d) gating response (I_{ds}–V_g) of the GaTe phototransistor in the dark and under illumination at 254 nm and 490 nm; (e) band diagram of a GaTe nanosheet phototransistor with a small Schottky barrier: E_F is the Fermi level energy, E_c the minimum conduction band energy, E_v maximum valence band energy and Φ_B the Schottky barrier height. The photocurrent is generated under illumination and is the dominant channel current in the OFF state while photoexcitation, thermionic and tunnelling currents contribute in the ON state of the device.

phototransistors can be explained by a simple energy band diagram (Fig. 3(e)). The GaTe device is in its equilibrium state without illumination and applied bias voltage, can be characterized by a small Schottky barrier. As the OFF state devices are illuminated ($V_g < V_t$), light absorption and excitations of hole–electron pairs occur, which can be extracted to generate photocurrent by applying a bias. The photocurrent increases with decreasing wavelength because the higher excitation energy provided by higher photon energies can produce more excitations. In the ON state ($V_g > V_t$), photoexcited current and the thermionic and tunneling currents all contribute to the device current. Decreasing gate voltage can lower the barriers at the contacts, resulting in more efficient photocurrent extraction and photoresponse increase.

Responsivity (R_λ) is the critical parameter for a photodetector, and is defined as the photocurrent generated per unit power of the incident light on the effective area of a photoconductor. R_λ can be calculated by $R_\lambda = \Delta I/PS$, where ΔI is the photoexcited current, P is the light power intensity irradiated on the GaTe nanosheet and S is the effective area of photodetector. Figure 4(a) shows the gate dependent responsivity (R_λ) which is acquired at bias voltage $V_{ds} = 2$ V under illumination of 490 nm and 254 nm. Responsivity

measured under the illumination of 490 nm (R_{490nm}) increases from 26.4 AW^{-1} at $V_g = 20$ V to 63.6 AW^{-1} at $V_g = -20$ V, while $R_{254\,nm}$ varied from 101.0 AW^{-1} at $V_g = 20$ V to 219.6 AW^{-1} at $V_g = -20$ V. Figure 4(b) shows the photocurrent and responsivity as function of illumination intensity. Photocurrent displays a significant increase with illumination intensity. The decrease in responsivity is due to the large quantity of traps at the interface between high surface-ratio GaTe and the underlying SiO_2 substrate. Under high illumination
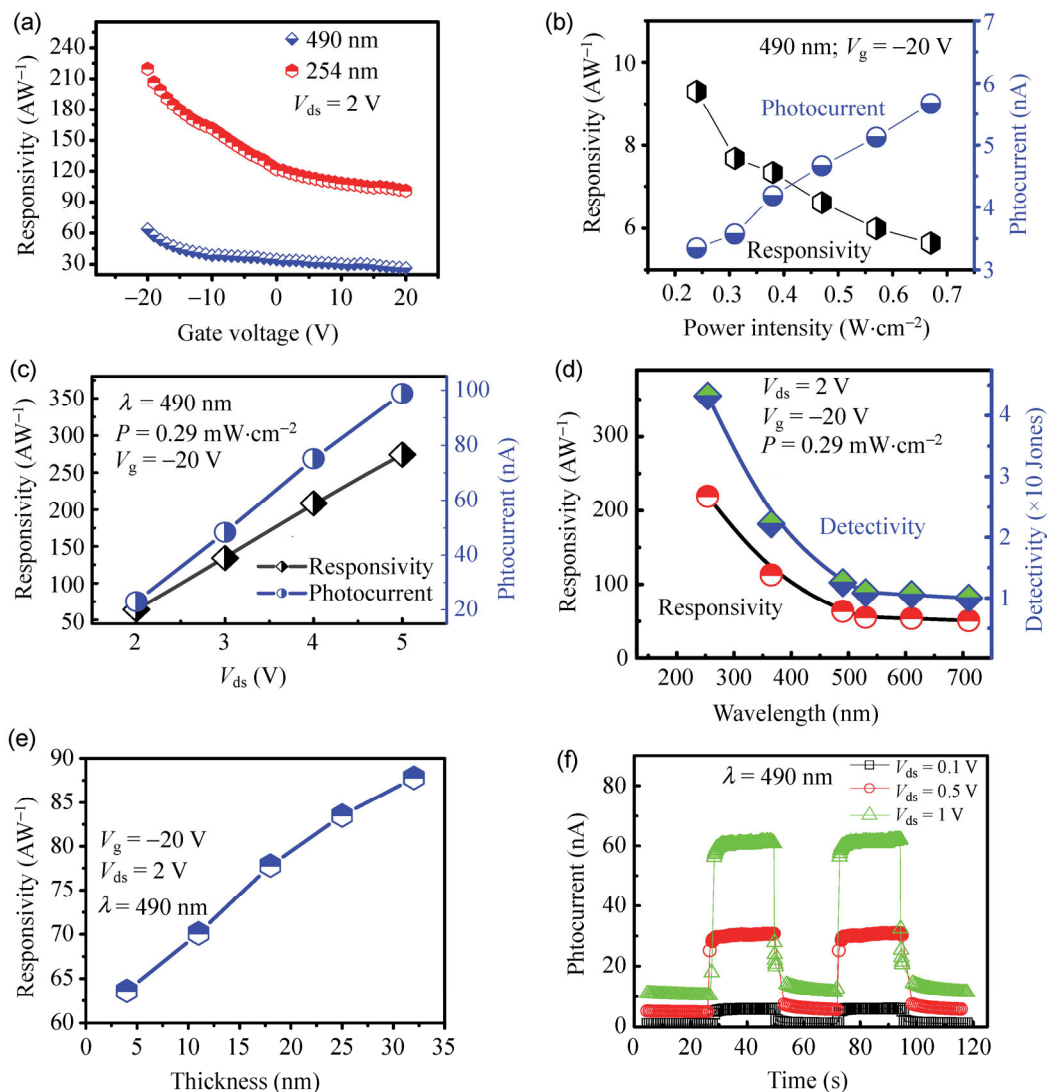

Figure 4 Photoresponse performance of the GaTe phototransistor. (a) Gate voltage dependent responsivity for bias voltage $V_{ds} = 2$ V and illumination intensity $P = 0.29$ mW·cm^{-1} under illumination wavelengths of 490 nm and 254 nm; (b) responsivity and photocurrent as function of illumination intensity under illumination wavelength of 490 nm at gate bias $V_g = -20$ V; (c) responsivity and photocurrent as function of drain bias voltage—the device exhibits a photosensitivity of 274.4 AW^{-1} for an illumination intensity of 0.29 mW·cm^{-2} at $V_g = -20$ V; (d) responsivity and detectivity under different illumination wavelengths; (e) responsivity as a function of thickness; (f) time-resolved photoresponse at different bias voltages $V_{ds} = 0.1$, 0.5, and 1 V.

intensity, the density of effective photoinduced states is decreased, which decreases the photoresponse. Under 490-nm illumination with an optimized intensity of 0.29 mW·cm^{-2} (Fig. 4(c)), the responsivity and photocurrent both show a linear dependence with varying source–drain bias V_{ds}, which corresponds well with the higher carrier drift velocities caused by applying larger bias. Responsivity of 274.4 AW^{-1} can be achieved at a source–drain voltage of V_{ds} = 5 V, and at a back gate voltage of V_g = –20 V, which is about ~10^6 times higher than the first graphene photodetectors [13]. This ultrahigh responsivity possibly originates from efficient light absorption and optimized device architecture. The photocurrent generation is strongly influenced by the thickness of the GaTe nanosheets (shown in Fig. 4(e)). Responsivity varied from 63.6 AW^{-1} with a 4 nm-thick GaTe to 87.8 AW^{-1} with a 32 nm-thick nanosheets when the device was illuminated under 490 nm light with an intensity of 0.29 mW·cm^{-2} by applying V_g = –20 V and V_{ds} = 2 V. Thicker nanosheets can absorb more photons, which can enhance the photocurrent inside the devices.

The sensitivity of the GaTe phototransistors is quantified by measurement of detectivity (D^*). Since the shot noise from the dark current is the major contribution to the total noise in our case, the detectivity can be given by D^* = $RA^{1/2}/(2eI_d)^{1/2}$, where R is the responsivity, A is the effective area of the detector, e is the absolute value of electron charge, and I_d is the dark current density [11]. Figure 4(d) shows the calculated D^* of the GaTe nanosheet photodetector on SiO$_2$/Si at different wavelengths. D^* is in the range of ~10^{12} Jones, which is comparable to existing InGaAs devices (D^* ~ 10^{12} Jones) [25]. This high detectivity arises from the high degree of electrostatic control over the ultrathin channel, the direct bandgap, and highly efficient excitation of GaTe.

Response time is another important parameter for a photodetectors. Figure 4(f) shows the time-resolved responses of GaTe phototransistors for three different source–drain voltages as UV illumination of 490 nm is turned on or off. The photoresponse is characterized by a typical rise time of τ_{rise} = 48 ms and a decay time of τ_{decay} = 150 ms. The rising and falling part of the curves can be fitted using a single exponential function:

$I(t) = I_{dark} + A\exp(t/\tau_{rise})$ and $I(t) = I_{dark} + A\exp(-t/\tau_{decay})$, where I_{dark} is the dark current, A is a scaling constant, and t is the time when the light is switched on or off. The photocurrent rise (τ_{rise}) and decay (τ_{decay}) observed in this study are similar to the corresponding values reported in GaSe nanosheet photodetectors [10]. These values are orders of magnitude shorter than those for phototransistors based on monolayer MoS$_2$ [19]. In previous demonstration, the dynamic response of the monolayer MoS$_2$ phototransistors was found to be closely related to the surroundings of the nanosheet due to its high surface ratio [17]. Future significant enhancement of photoresponse time for GaTe nanosheet transistors could be realized by surface trap state passivation.

The performance parameters of the GaTe nanosheet photodetectors are compared to other reported 2D nanosheet photodetectors (Table S1 in the Electronic Supplementary Material (ESM)). Graphene photodetectors show a low responsivity of 10^{-3} AW^{-1}, whilst GaSe and GaS devices have responsivities of 2.8 AW^{-1} and 4.2 AW^{-1}, respectively. GaTe nanosheet photodetectors show a responsivity of 274.4 AW^{-1} which is much higher than the values reported for 2D nanosheet devices including GaSe and GaS [10, 11, 15]. GaTe optoelectronics also have a faster response time than single-layer MoS$_2$ photodetectors [19]. Although a higher value of 880 AW^{-1} has been achieved with monolayer MoS$_2$ devices using treated SiO$_2$/Si and a large gate voltage of –70 V [19], the slow response of 4 s limits its application. We attribute the exceptionally high photoresponse of GaTe to its relativity small direct bandgap of ~1.60 eV, the smallest among all those reported 2D layer materials. All of these results indicate that GaTe nanosheets are promising for use in highly sensitive nanoscale photodetectors.

To reveal the origin of the ultrahigh photoresponse in 2D GaTe nanosheets, we performed first-principles quantum mechanical calculations to understand the electronic structure of 2D GaTe nanosheets. We employed projector-augmented wave potentials and exchange-correlation potentials of the Perdew–Burke–Ernzerhof (PBE) [34] version of the generalized-gradient approximation (GGA), as implemented in the Vienna *ab initio* simulation package (VASP) [35].

The experimentally observed nanosheets were theoretically modeled as a slab consisting of two GaTe layers in a supercell, where the atomic arrangement of in-planar layer directions (*a* and *c* directions) are infinitely repeating and the layer stacked direction (*b* direction) has a sufficiently large empty space ("vacuum" of ~30 Å) to avoid any artificial interactions between the neighboring cells in *b*-direction. For an accurate total energy calculations of the supercell, $11 \times 1 \times 11$ number of k-points in each direction was used. The atomistic structure of GaTe nanosheet is displayed in Fig. 5(a). Figure 5(b) shows the Brillouin zone of the 2D nanosheet and high symmetry k-points. The bandgap structures of GaTe nanosheets varies with the thickness, the nanosheets with more than two layers show a direct bandgap, and a crossover from direct to indirect bandgap appears when the thickness is reduced to two layers. Actually, the indirect bandgap of one- or two-layer-GaTe should be of a quasi-direct character due to the very small shift of the valence band maximum (VBM) from the Γ point. The energy band structures of one monolayer (1 ML) nanosheets is displayed in Fig. 5(c), which shows a quasi-direct bandgap with the valence band maximum is located at the Γ. In Fig. S1 (in the ESM), the gap changes from ~1.58 eV for 1 ML to ~1.09 eV for 4 ML. The dotted line is for the bulk gap (E_g = ~1.0 eV). From 2 ML there is an indirect bandgap but thin layers up to 4 ML can still be called quasi-direct gap materials. The direct bandgap of GaTe nanosheets endows them with a strong

capability for light absorption and thus generation of photoexcitants.

4 Conclusion

We have characterized 2D GaTe nanosheets and fabricated phototransistors based on few-layer GaTe nanosheets. The performance of photodetectors based upon GaTe ultrathin layers can be effectively controlled by applying a gate bias. Because of the direct bandgap of GaTe nanosheets, the devices exhibit an ultrahigh photoresponsivity of 274.3 AW^{-1} and ultrahigh detectivity of ~4 × 10^{12} Jones at a wavelength of 490 nm. The 2D GaTe photodetector could be potentially integrated into various optical sensors that require a broad range of spectral responses from UV to visible light. The theoretical model shows that the direct bandgap structure makes 2D GaTe nanosheets a promising material for use in optoelectronics. Therefore, our highly sensitive GaTe nanosheet phototransistors can be attractive for various applications in touch sensor panels, image sensors and solar cells.
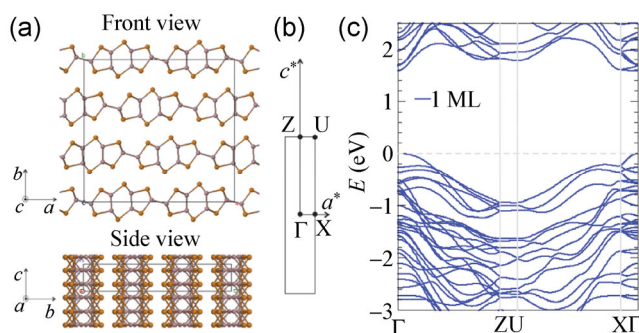
Figure 5 (a) The structures of GaTe layers, where the bulk unit cell is depicted as solid lines. (b) Brillouin zone of two-dimensional materials stacked along the *b* direction. (c) Electronic band of 1 ML (ML, monolayer) along the in-plane high-symmetry points shown in (b), where the energy levels are with respect to the valence band maximum (indicated as the dotted vertical line) located at the Γ point.

Electronic Supplementary Material: Supplementary material is available in the online version of this article at http://dx.doi.org/10.1007/s12274-014-0430-2.

References

[1] Geim, A. K.; Grigorieva, I. V. Van der Waals heterostructure. *Nature* **2013**, *499*, 419–425.

[2] Tang, Q.; Zhou, Z. Graphene-analogous low-dimensional materials. *Prog. Mater. Sci.* **2013**, *58*, 1244–1315.

[3] Huang, X.; Zeng, Z. Y.; Zhang, H. Metal dichalcogenide nanosheets: Preparation, properties and applications. *Chem. Soc. Rev.* **2013**, *42*, 1934–1946.

[4] Chhowalla, M.; Shin, H. S.; Eda, G.; Li, L. J.; Loh, K. P.; Zhang, H. The chemistry of two-dimensional layered transition metal dichalcogenide nanosheets. *Nat. Chem.* **2013**, *5*, 263–275.

[5] Zeng, Z. Y.; Yin, Z. Y.; Huang, X.; Li, H.; He, Q. Y.; Lu, G.; Boey, F.; Zhang, H. Single-layer semiconducting nanosheets: High-yield preparation and device fabrication. *Angew. Chem. Int. Ed.* **2011**, *50*, 11093–11097.

[6] He, Q. Y.; Zeng, Z. Y.; Li, H.; Wu, S. X.; Huang, X.; Zhang, H. Fabrication of flexible MoS_2 thin-film transistor arrays for practical gas-sensing applications. *Small* **2012**, *8*, 2994–2999.

[7] Wu, J.; Li, H.; Yin, Z. Y.; Li, H.; Liu, J. Q.; Cao, X. H.; Zhang, Q.; Zhang, H. Layer thinning and etching of mechanically exfoliated MoS_2 nanosheets by thermal annealing in air. *Small* **2013**, *9*, 3314–3319.

[8] Yin, Z. Y.; Li, H.; Li, H.; Jiang, L.; Shi, Y. M.; Sun, Y. H.; Lu, G.; Zhang, Q.; Chen, X. D.; Zhang, H. Single-layer MoS_2 phototransistors. *ACS Nano* **2012**, *6*, 74–80.

[9] Zhang, Y.; Zhang, Y. F.; Ji, Q. Q.; Ju, J.; Yuan, H. T.; Shi, J. P.; Gao, T.; Ma, D. L.; Liu, M. X.; Chen, Y. B., et al. Controlled growth of high-quality monolayer WS_2 layers on sapphire and imaging its grain boundary. *ACS Nano* **2013**, *7*, 8963–8971.

[10] Hu, P. A.; Wen, Z. Z.; Wang, L. F.; Tan, P. H.; Xiao, K. Synthesis of few-layer GaSe nanosheets for high performance photodetectors. *ACS Nano* **2012**, *6*, 5988–5994.

[11] Hu, P. A.; Wang, L. F.; Yoon, M.; Zhang, J.; Feng, W.; Wang, X. N.; Wen, Z. Z.; Idrobo, J. C.; Miyamoto, Y.; Geohegan, D. B.; Xiao, K. Highly responsive ultrathin GaS nanosheet photodetectors on rigid and flexible substrates. *Nano Lett.* **2013**, *13*, 1649–1654.

[12] Lin, M.; Wu, D.; Zhou, Y.; Huang, W.; Jiang, W.; Zheng, W. S.; Zhao, S. L.; Jin, C. H.; Guo, Y. F.; Peng, H. L., et al. Controlled growth of atomically thin In_2Se_3 flakes by van der Waals epitaxy. *J. Am. Chem. Soc.* **2013**, *135*, 13274–13277.

[13] Zhou,Y. B.; Nie,Y. F.; Liu,Y. J.; Yan, K.; Hong, J. H.; Jin, C. H.; Zhou, Y.; Yin, J. B.; Liu, Z. F.; Peng, H. L. Epitaxy and photoresponse of two-dimensional GaSe crystals on flexible transparent mica sheets. *ACS Nano*, in press, DOI: 10.1021/nn405529r.

[14] Nair, R. R.; Blake, P.; Grigorenko, A. N.; Novoselov, K. S.; Booth, T. J.; Stauber, T.; Peres, N. M. R.; Geim, A. K. Fine structure constant defines visual transparency of graphene. *Science* **2008**, *320*, 1308.

[15] Xia, F. N.; Mueller, T.; Lin, Y. M.; Valdes-Garcia, A.; Avouris, P. Ultrafast graphene photodetector. *Nat. Nanotechnol.* **2009**, *4*, 839–843.

[16] Gan, X. T.; Shiue, R. J.; Gao, Y. D.; Meric, I.; Heinz, T. F.; Shepard, K.; Hone, J.; Assefa, S.; Englund, D. Chip-integrated ultrafast graphene photodetector with high responsivity. *Nat. Photonics* **2013**, *7*, 883–887.

[17] Khan, M. A.; Kuznia, J. N.; Olson, D. T.; Blasingame, M.; Bhattarai, A. R. Schottky barrier photodetector based on Mg-doped p-type GaN films. *Appl. Phys. Lett.* **1993**, *63*, 2455–2456.

[18] Zhang, Y. Z.; Liu, T.; Meng, B.; Li, X. H.; Liang, G. Z.; Hu, X. N.; Zhang, Q. J. Broadband high photoresponse from pure monolayer graphene photodetector. *Nat. Commun.* **2013**, *4*, 1811.

[19] Lopez-Sanchez, O.; Lembke, D.; Kayci, M.; Radenovic, A.; Kis, A. Ultrasensitive photodetectors based on monolayer MoS_2. *Nat. Nanotechnol.* **2013**, *8*, 497–501.

[20] Ji, Q. Q.; Zhang, Y. F.; Gao, T.; Zhang, Y.; Ma, D. L.; Liu, M. X.; Chen, Y. B.; Qiao, X. F.; Tan, P. H.; Kan, M., et al. Epitaxial monolayer MoS_2 on mica with novel photoluminescence. *Nano Lett.* **2013**, *13*, 3870–3877.

[21] Najmaei, S.; Liu, Z.; Zhou, W.; Zou, X. L.; Shi, G.; Lei, S. D.; Yakobson, B. I.; Idrobo, J. C.; Ajayan, P. M.; Lou, J. Vapour phase growth and grain boundary structure of molybdenum disulphide atomic layers. *Nat. Mater.* **2013**, *12*, 753–759.

[22] Genut, M.; Margulis, L.; Hodes, G.; Tenne, R. Preparation and microstructure WS_2 thin films. *Thin Solid Films*, **1992**, *217*, 91–97.

[23] Leão, C. R.; Lordi, V. *Ab initio* guided optimization of GaTe for radiation detection applications. *Phys. Rev. B* **2011**, *84*, 165206.

[24] Bose, D. N.; Pal, S. Photoconductivity, low-temperature conductivity, and magnetoresistance studies on the layered semiconductor GaTe. *Phys. Rev. B* **2001**, *63*, 235321.

[25] Mandal, K. C.; Krishna, R. M.; Hayes, T. C.; Muzykov, P. G.; Das, S.; Sudarshan, T. S.; Ma, S. G. Layered GaTe crystals for radiation detectors. *IEEE Trans. Nucl Sci.* **2011**, *58*, 1981–1986.

[26] Julien, C.; Ivanov, I.; Ecrepont, C.; Guittard, M. Optical and electrical properties of Ga_2Te_3 crystals. *Phys. Statu. Solidi (a)* **1994**, *145*, 207–215.

[27] Konstantatos, G.; Howard, I.; Fischer, A.; Hoogland, S.; Clifford, J.; Klem, E.; Levina, L.; Sargent, E. H. Ultrasensitive solution-cast quantum dot photodetectors. *Nature* **2006**, *442*, 180–183.

[28] Loudon, R. The Raman effect in crystals. *Adv. Phys*. **2001**, *50*, 813–864.

[29] Lee, C.; Yan, H.; Brus, L. E.; Heinz, T. F.; Hone, J.; Ryu, S. Anomalous lattice vibrations of single- and few-layer MoS_2. *ACS Nano* **2010**, *4*, 2695–2700.

[30] Late, D. J.; Liu, B.; Matte, H. S. S. R.; Rao, C. N. R.; Dravid, V. P. Rapid characterization of ultrathin layers of chalcogenides on SiO_2/Si substrates. *Adv. Funct. Mater.* **2012**, *22*, 1894–1905.

[31] Harper, P. G.; Hilder, J. A. Exciton spectra in thin crystals. *Phys. Status Solidi (b)*. **1968**, *26*, 69–76.

[32] Radisavljevic, B.; Radenovic, A.; Brivio, J.; Giacometti, V.; Kis, A. Single-layer MoS_2 transistors. *Nat. Nanotechnol.* **2011**, *6*, 147–150.

[33] Late, D. J.; Liu, B.; Luo, J. J.; Yan, A. M.; Matte, H. S. S. R.; Grayson, M.; Rao, C. N. R.; Dravid, V. P. GaS and GaSe ultrathin layer transistors. *Adv. Mater.* **2012**, *24*, 3549–3554.

[34] Perdew, J. P.; Burke, K.; Ernzerhof, M. Generalized gradient approximation made simple. *Phys. Rev. Lett*. **1996**, *77*, 3865–3868.

[35] Kresse, G.; Joubert, D. From ultrasoft pseudopotentials to the projector augmented-wave method. *Phys. Rev. B* **1999**, *59*, 1758–1775.